Article

Electrochemical Property: Structure Relationships in Monoclinic LiV(PO)

S.-C. Yin, H. Grondey, P. Strobel, M. Anne, and L. F. Nazar

J. Am. Chem. Soc., **2003**, 125 (34), 10402-10411• DOI: 10.1021/ja034565h • Publication Date (Web): 31 July 2003

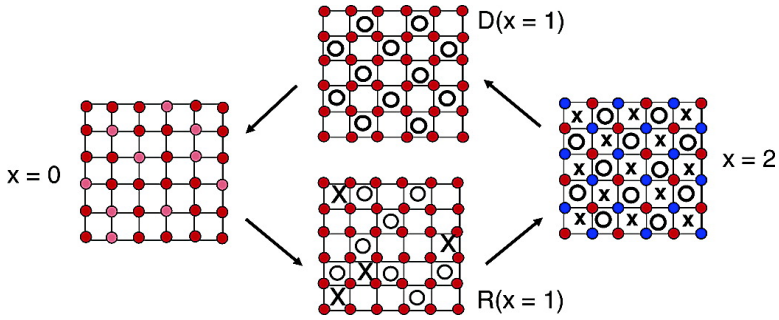

More About This Article

Additional resources and features associated with this article are available within the HTML version:

- Supporting Information
- Links to the 6 articles that cite this article, as of the time of this article download
- Access to high resolution figures
- Links to articles and content related to this article
- Copyright permission to reproduce figures and/or text from this article

View the Full Text HTML

J|A|C|S
ARTICLES
Published on Web 07/31/2003

Electrochemical Property: Structure Relationships in Monoclinic $Li_{3-y}V_2(PO_4)_3$

S.-C. Yin,[†] H. Grondey,[‡] P. Strobel,[§] M. Anne,[§] and L. F. Nazar*,[†]

Contribution from the Department of Chemistry, University of Waterloo, Waterloo, Ontario, Canada N2L 3G1, Department of Chemistry, NMR Facility, University of Toronto, and CNRS, Laboratoire de Cristallographie, Grenoble, France

Received February 7, 2003; E-mail: lfnazar@uwaterloo.ca

Abstract: Monoclinic lithium vanadium phosphate, α-$Li_3V_2(PO_4)_3$, is a highly promising material proposed as a cathode for lithium-ion batteries. It possesses both good ion mobility and high lithium capacity because of its ability to reversibly extract all three lithium ions from the lattice. Here, using a combination of neutron diffraction and ^{7}Li MAS NMR studies, we are able to correlate the structural features in the series of single-phase materials $Li_{3-y}V_2(PO_4)_3$ with the electrochemical voltage−composition profile. A combination of charge ordering on the vanadium sites and lithium ordering/disordering among lattice sites is responsible for the features in the electrochemical curve, including the observed hysteresis. Importantly, this work highlights the importance of ion−ion interactions in determining phase transitions in these materials.

Introduction

The advent of new crystalline lattices capable of reversible lithium intercalation is of perpetual interest in solid-state materials chemistry. These materials also find use as electrodes in lithium-ion energy storage devices.[1] The field, however, remains plagued by the inability to implement materials that can compete with the highly successful $LiCoO_2$, despite its detriments including high cost which prohibit its use in large-scale devices. A tremendous resurgence of interest has been displayed in lithium metal phosphates, sparked by recent reports of the promising characteristics of $LiFePO_4$,[2] $LiMnPO_4$,[3] $Li_3V_2(PO_4)_3$,[4] and related compounds.[5] These materials contain both mobile Li cations and redox-active metal sites shrouded within a rigid phosphate network. By comparison to lithium metal oxides, they display remarkable electrochemical and thermal stability, and comparable energy density.[6] The iron phosphate is an inexpensive, relatively high capacity material that may find a niche in hybrid electric vehicles,[7] whereas reversible extraction of all three lithium ions from the monoclinic vanadium phosphate at slow,[8] and even at very fast rates,[9] results in the highest energy density metal phosphate reported to date.

Fewer breakthroughs have been reported in understanding the factors governing their electrochemical response. Fundamentally, these materials present many questions that relate to the transport of electrons and lithium ions within the lattice. Even more intriguing is the origin of two-phase transitions that signal compositional changes during the redox processes that accompany electrochemical lithium extraction/insertion within the material. Often the fully lithiated and delithiated frameworks that span a phase transition are very similar, raising the question of why solid solution behavior is not observed. Such questions have impact on the vanadium phosphate under study here, as well as other metal phosphates that display similar two-phase behavior such as $LiFePO_4$. The understanding of such physical phenomena is critical to the search for new materials, as well as improvements in the current ones.

The title material, $Li_3V_2(PO_4)_3$, exists in two different phases: the thermodynamically more stable monoclinic form[10] and the rhombohedral or NASICON phase that is only accessible *via* ion-exchange of the corresponding sodium phase.[11] The two materials display very different voltage−composition curves as a result of their structural differences. The latter displays one plateau resulting from a two-phase transition between the compositions $Li_3V_2(PO_4)_3$ and $Li_1V_2(PO_4)_3$.[12] This corresponds to extraction of two Li from a single tetrahedrally coordinated

[†] University of Waterloo.
[‡] University of Toronto.
[§] CNRS.

(1) Thackeray, M. M.; Thomas, J. O.; Whittingham, M. S. *MRS Bull.* **2000**, *25*, 39.
(2) Padhi, A. K.; Nanjndaswamy, K. S.; Goodenough, J. B. *J. Electrochem. Soc.* **1997**, *144*, 1188. Huang, H.; Yin, S.-C.; Nazar, L. F. *Electrochem. Solid- State Lett.* **2001**, *4*, A170.
(3) Li, G.; Azuma, H.; Tohda, M. *Electrochem. Solid-State Lett.* **2002**, *5*, A135.
(4) Saïdi, M. Y.; Barker, J.; Huang, H.; Adamson, G. U.S. Patent 5871866, 1999.
(5) Padhi, A. K.; Manivannan, K. S. V.; Goodenough, J. B. *J. Electrochem. Soc.* **1998**, *145*, 1518. Nanjundaswamy, K. S.; Padhi, A. K.; Goodenough, J. B.; Okada, S.; Ohtsuka, H.; Arai, H.; Yamaki, J. *Solid State Ionics* **1996**, *92*, 1.
(6) Yamada, A.; Chung, S. C.; Hinokuma, K. *J. Electrochem. Soc.* **2001**, *148*, A224.
(7) Goodenough, J. B.; Padhi, A. K.; Nanjundaswamy, K. S.; Masquelier, C. U.S. Patent 5910382, 1999. Ravet, N.; Goodenough, J. B.; Besner, S.; Simoneau, M.; Hovington, P.; Armand, M. Abstract #127, 196th ECS Meeting; Honolulu, HI; The Electrochemical Society: Pennington, NJ, 1999.
(8) Saïdi, M. Y.; Barker, J.; Huang, H.; Adamson, G. *Electrochem. Solid-State Lett.* **2002**, *5*, A149.
(9) Huang, H.; Yin, S.-C.; Kerr, T.; Nazar, L. F. *Adv. Mater.* **2002**, *14*, 1525.
(10) Ohkawa, H.; Yoshida, K.; Saito, M.; Uematsu, K.; Toda, K.; Sato, M. *Chem. Lett.* **1999**, 1017.
(11) Masquelier, C.; Wurm, C.; Rodriguez-Carvajal, J.; Gaubicher, J.; Nazar, L. *Chem. Mater.* **2000**, *12*, 525−532.
(12) Gaubicher, J.; Goward, G.; Wurm, C.; Masquelier, C.; Nazar, L. F. *Chem. Mater.* **2000**, *12*, 3240.

10.1021/ja034565h CCC: $25.00

site and displacement of the remaining Li to another site. The monoclinic phase, where all three Li are mobile, exhibits a particularly complex series of two-phase transitions on lithium extraction, followed by a solid solution regime on lithium reinsertion.[9] On the subsequent extraction curve, the cycle is repeated. Our preliminary report, concerned with lithium extraction, demonstrated that the underlying physical phenomena that give rise to the two-phase transitions involve lithium reordering.[13] Here, we describe the subtle interplay between structure and electrochemical properties in the full electrochemical curve on oxidation (Li extraction) and reduction (Li insertion). We reveal that the unusual hysteresis observed between extraction and reinsertion of lithium into this structure results from disruption of vanadium charge ordering in the fully delithiated phase. This leads to solid solution behavior on lithium reinsertion. Our findings have implications for understanding charge transport in these materials, and in developing other metal phosphates that display solid solution behavior.

Experimental Section

Sample Preparation. Microcrystalline α-$Li_3V_2(PO_4)_3$ was prepared by mixing stoichiometric amounts of Li_2CO_3 (Aldrich, 99.99%), V_2O_5 (99.6%), and $NH_4H_2PO_4$ (99.99%). The mixture was heated at 300 °C for 3 h, reground, and fired at 850 °C for 12 h under a flow of 7% H_2/N_2. Chemical oxidation/reduction methods were used to obtain bulk quantities of $Li_xV_2(PO_4)_3$ samples for neutron diffraction measurements. The $x = 2.5$, 2.0, 1.0, and 0.0 compositions were prepared by stoichiometric chemical oxidation of α-$Li_3V_2(PO_4)_3$ with 1 M $NOBF_4$ or NO_2BF_4 in acetonitrile for 24 h in an Ar-filled glovebox to reach the desired lithium content (deinsertion, denoted "D"). Reinserted samples $x = 0.50-1.5$, 2, 3 (reinsertion, denoted "R") were prepared by stoichiometric reaction of the $V_2(PO_4)_3$ phase with LiI. The products in each case were filtered and washed with acetonitrile three times to remove remaining salts. To ensure the prepared materials were of the correct stoichiometry, their open-circuit voltage was measured versus Li^+/Li. A short oxidation or reduction step (Δx (Li) ≈ 0.1) revealed the presence of the desired single-phase composition through examination of the change in the slope of the voltage−composition curve. The samples obtained were structurally similar to those obtained electrochemically, as was proven by the identical X-ray diffraction patterns recorded for selected samples, including that of α-$Li_3V_2(PO_4)_3$ following Li extraction and reinsertion. The delithiated materials were subjected to chemical analysis to confirm the Li/V ratio.[14]

Powder Neutron Diffraction. About 2 g of each sample was loaded in a vanadium can in an Ar-filled glovebox. Initial neutron diffraction experiments were carried out on the C2 diffractometer at the Chalk River Laboratories, Ottawa, Canada ($\lambda = 1.3291$ Å). Subsequent studies were performed on the D2B high-resolution diffractometer at the Institut Laue-Langevin (ILL), Grenoble ($\lambda = 1.5940$ Å); data were collected from 6 to 12 h over the range $2\theta = 10-160°$, with a step size of 0.05°. The latter data sets were used for the final structural refinements except for $x = 3$.

Powder X-ray Diffraction. Samples were measured on a Siemens D500 powder diffractometer ($\lambda = 1.5405$Å) from $2\theta = 10-100°$ at a count rate of 10 s per step of 0.02°.

LeBail Pattern Matching and Rietveld Refinement. Refinements were performed using GSAS software.[15] The cell parameters of each delithiated phase were first determined by LeBail pattern matching. Subsequent Rietveld refinement analysis was carried out initially using fractional coordinates from our single-crystal $Li_3V_2(PO_4)_3$ analysis.[9] Scale factor, zero point, lattice parameters, atomic positions, and thermal factors were iteratively refined (see Supporting Information for details). The vanadium positions were based on an initial combined X-ray and neutron refinement and were kept fixed during the final stages of the neutron refinement. The X-ray data were not included at this stage as the refinement was improved without it. The thermal parameter for vanadium was kept fixed during the refinement, and thermal factor constraints were applied to P, O, and Li atoms separately.

^{7}Li MAS NMR Measurements. Samples were hermetically sealed in zirconia rotors fitted with airtight Kel-F caps in an Ar-filled glovebox. The spectra were recorded on a Bruker DSX200 spectrometer at the resonance frequency of ^{7}Li (77.789 MHz). Lithium lactate was used as the reference (0 ppm). To acquire the spectra, a single pulse sequence was used with a 2.5 μs (90°) pulse length and a repetition time of 2 s. The spinning speeds were varied from 6 to11.5 kHz to identify the isotropic chemical shifts. For the temperature-dependent experiment, the sample was heated between 294 and 334 K at 10 K intervals. The spectral peak area integration was calculated by the DmFit program.[16]

Electrochemistry Measurements. Electrochemical cells were constructed using a Swagelok design, utilizing 1 M $LiPF_6$/EC-DMC (Merck) as the electrolyte. The cathodes were comprised of a $Li_3V_2(PO_4)_3$/C composite (15% carbon), Super S (MMM), and PVDF binder with the weight ratio 85:10:5. Cells were assembled in a glovebox under Ar with O_2 and H_2O lower than 5 ppm. Samples were examined in the galvanostatic intermittent titration mode with a current pulse equivalent to a C/5 rate (approximately 0.1 mA for 0.5 h, for an 8 mg electrode). Each step was followed by relaxation under open circuit conditions until the potential change was less than 2 mV/h or the relaxation time exceeded 0.5 h.

Results and Discussion

(1) The Electrochemical Voltage−Composition Curve of Monoclinic $Li_3V_2(PO_4)_3$: General Features. The monoclinic $Li_3M_2(PO_4)_3$ phases are only slightly more dense than their well-known fast-ion conducting rhombohedral NASICON analogues, suggesting that ion mobility within monoclinic $Li_3V_2(PO_4)_3$ should be relatively facile.[17] Electronic transport, however, is somewhat limited in all lithium metal phosphates, because of the presence of the $(PO_4)^{3-}$ groups. These have the crucial benefit of raising the redox potential to practical values, but at the expense of localizing the d-electron bands. Our four-probe conductivity measurements on pressed pellets of pale green $Li_3V_2(PO_4)_3$ show a conductivity of 2×10^{-8} S/cm, typical of other lithium metal phosphates such as $LiFePO_4$.[18] Nonetheless, all three lithium ions can be electrochemically extracted from the framework and reversibly reinserted. In conventional electrochemical electrodes, low current densities are required.[8] We have attained full reversible extraction at very fast rates, by nucleation and restricted growth of small $Li_3V_2(PO_4)_3$ crystallites within a conductive-carbon matrix.[9] Both these fast and slow rate experiments and our galvanostatic intermittent titration experiments (GITT) which utilize a relaxation period to maintain the system at quasi-equilibrium[13] have demonstrated that the plateaus in the oxidation curve correspond to a sequence of transitions between single phases in $Li_xV_2(PO_4)_3$, comprised of $x = 2.5$ (i); 2.0 (ii); 1.0 (iii); 0.0 (iv). These phases, which

(13) Yin, S. C.; Grondey, H.; Strobel, P.; Huang, H.; Nazar, L. F. *J. Am. Chem. Soc.* **2003**, *125*, 326.
(14) Li:V ratios were determined by chemical analysis (ICP): $Li_3V_2(PO_4)_3$, 2.88; $Li_2V_2(PO_4)_3$, 1.80; $Li_1V_2(PO_4)_3$, 0.82; $V_2(PO_4)_3$, 0.15; R-$Li_1V_2(PO_4)_3$, 1.03.
(15) Larson, A. C.; Dreele, R. B. V. GSAS; Technical Report NM87545; Los Alamos National Laboratory: Los Alamos, NM, 1994.
(16) Massiot, D.; Fayon, F.; Capron, M.; King, I.; Le Calvé, S.; Alonso, S.; Durand, J.-O.; Bujoli, B.; Gan, Z.; Hoatson, G. *Magn. Reson. Chem.* **2002**, *40*, 70−76.
(17) Padhi, A. K.; Nanjundaswamy, K. S.; Masquelier, C.; Goodenough, J. B. *J. Electrochem. Soc.* **1997**, *144*, 2581. Padhi, A. K.; Manivannan, V.; Goodenough, J. B. *J. Electrochem. Soc.* **1998**, *145*, 1518.
(18) Chung, S. Y.; Bloking, J. T.; Chiang, Y. M. *Nat. Mater.* **2002**, *1*, 123.

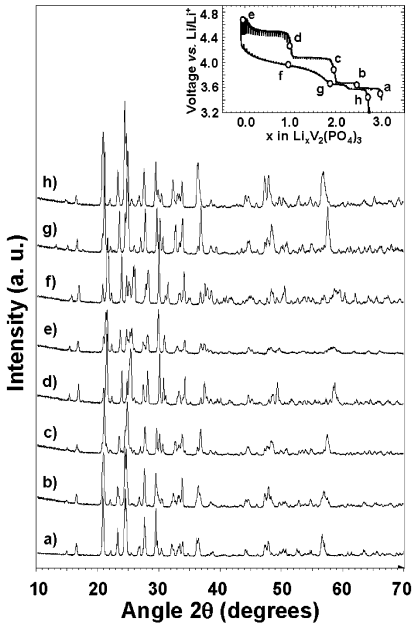

Figure 1. XRD diffraction patterns for (a) $x = 3$, starting phase; (b) $x = 2.5$, deinsertion; (c) $x = 2$, deinsertion; (d) $x = 1$, deinsertion; (e) $x = 0$; (f) $x = 1$, reinsertion; (g) $x = 2$, reinsertion; (h) $x = 3$, reinsertion. Inset: Galvanostatic intermittent titration (GITT) plot, reproduced from ref 13, for Li extraction from $Li_3V_2(PO_4)_3$ illustrating the location of the single-phase compositions $Li_xV_2(PO_4)_3$ ($x = 3.0 \rightarrow 0.0$, see text), followed by Li insertion. Note the solid solution behavior present between $x = 0$ and $x = 2$ even under "equilibrium" conditions.

have also been predicted by first-principles calculations,[19] are shown on the inset GITT electrochemical curve in Figure 1. Regions with a short pulse recovery time indicate fast equilibration. Extraction of the third Li ion/electron is the most kinetically hindered, as is shown by the increased time needed for relaxation in the region between $x = 1$ and 0. Most significant is the characteristic S-shaped curve displayed between $x = 0$ and $x = 2$ on reinsertion, an electrochemical signature of solid solution behavior. After the reinsertion of 2Li, however, the onset of two-phase behavior reappears. The process is completely reversible on the second cycle, as was previously demonstrated in fast-rate cycling experiments.[9]

Further confirmation of the reversibility of the extraction−insertion process comes from X-ray diffraction experiments on the single phases, shown in Figure 1. The XRD patterns of the $x = 3$ phase at the start (Figure 1a) and completion of one cycle (Figure 1h) are effectively identical, as are the XRD patterns of the $x = 2$ phases on deinsertion and reinsertion (Figure 1c,g). Notable, though, is the difference in the diffraction patterns between the two-phase transition region and the solid solution regime. The XRD pattern of the $x = 1$ phase on deinsertion (Figure 1d) is clearly different than the pattern of the reinserted $x = 1$ phase (Figure 1f). A slight loss of crystallinity observed in the $x = 0$ phase on full lithium extraction (Figure 1e) was observed. This was also noted in another study, although our data suggest the loss is less dramatic than was previously reported.[8] On reinsertion, the XRD (and neutron) patterns indicate that crystallinity is largely regained.

To understand the nature of these transitions, we carried out powder neutron diffraction (PND) experiments to locate the Li ions in the frameworks in the single phases and solid solution regime. These studies were coupled with solid-state ^{7}Li NMR investigations. Deinserted ("D") $x = 2.5$, 2.0, 1.0, and 0.0 single-phase compositions for this study were prepared by stoichiometric chemical oxidation of $Li_3V_2(PO_4)_3$ as described above, and reinserted samples ("R") were prepared by stoichiometric reaction of the $V_2(PO_4)_3$ phase with LiI. This provided large quantities of single-phase compositions needed for PND, free of binder and electrolyte that could compromise the neutron diffraction data due to incoherent scattering from protons or that could interfere with the ^{7}Li NMR patterns due to Li^+ contamination from the electrolyte.

The lattice parameters for each single phase were first determined by a full-pattern (LeBail) fit of the data, followed by Rietveld refinement of the experimental pattern without any Li atoms in the lattice. After the Li positions were located by difference Fourier mapping, the refinement was completed with the inclusion of these sites. All Rietveld fits converged satisfactorily with good statistics and little residual in the difference curve. For convenience, the refinement summaries for all phases are listed in Table 1. The details of the refinements, fractional coordinates, and bond lengths/angles are summarized in the Supporting Information.

(2) Extraction of Lithium (Oxidation Curve): Structure Descriptions and NMR. D-$Li_{3.0}V_2(PO_4)_3$. The structure of the title monoclinic phase $Li_3V_2(PO_4)_3$ based on single-crystal structure analysis[9] is isotypic with the iron phase $Li_3Fe_2(PO_4)_3$ reported by Bykov et al.[20] Refinement of the structure was also carried out using Rietveld analysis of the low-resolution neutron diffraction pattern. Because V is a very weak neutron scatterer, its atomic positions were refined using Rietveld analysis of the XRD pattern and were fixed at those values. Refinement of the Li, O, and P atomic positions converged to yield results essentially the same as those of the single-crystal analysis, with an agreement factor $R_{wp} = 4.32\%$ (see Table 1). The structure shown in Figure 2a-i depicts the $V_2(PO_4)_3$ framework and the three Li ions that reside in quasi-tetrahedral interstitial sites within the lattice.

The structure is related to, but slightly more dense than, the NASICON polytype of $Li_3V_2(PO_4)_3$.[12,21] The two vanadium sites V(1) and V(2) represent virtually identical slightly distorted VO_6 octahedra with average V−O bond lengths of 2.003 and 2.006 Å, and vanadium valencies of close to +3 based on bond-sum calculations (Table 2).[9] They are crystallographically distinguishable due to the monoclinic symmetry of this $P2_1/n$ lattice, although in the high-temperature orthorhombic γ-phase of $Li_3V_2(PO_4)_3$, they are not.[22] The three distinct lithium sites consist of one tetrahedral site, Li_1, in addition to two pseudotetrahedral sites. The latter (Li_2 and Li_3) environments exhibit an additional

(19) Morgan, D.; Ceder, G.; Saidi, Y.; Barker, J.; Swoyer, J.; Huang, H.; Adamson, G. *Chem. Mater.* **2002**, *14*, 4684. Morgan, D.; Ceder, G.; Saidi, Y.; Barker, J.; Swoyer, J.; Huang, H.; Adamson, G. *J. Power Sources*, in press. We note that they predict lattice sites similar to those we report here and previously in ref 13, although there are differences in lattice symmetry and coordination environments in some cases.

(20) Bykov, A. B.; Chirkin, A. P.; Demyanets, L. N.; Doronin, S. N.; Genkina, E. A.; Ivanov-Shits, A. K.; Kondratyuk, I. P.; Maksimov, B. A.; Mel'Nikov, O. K.; Muradyan, L. N.; Simonov, V. I.; Timofeeva, V. A. *Solid State Ionics* **1990**, *38*, 31. Note that sites Li_2 and Li_3 in $Li_3V_2(PO_4)_3$ are switched in our study by comparison to this reference.

(21) Nanjundaswamy, K. S.; Padhi, A. K.; Goodenough, J. B.; Okada, S.; Ohtsuka, H.; Arai, H.; Yamaki, J. *Solid State Ionics* **1996**, *92*, 1−10.

(22) Ohkawa, H.; Yoshida, K.; Saito, M.; Uematsu, K.; Toda, K.; Sato, M. *Chem. Lett.* **1999**, 1017. Sato, M.; Ohkawa, K.; Yoshida, K.; Saito, M.; Uematsu, K.; Toda, K. Paper A-19, 12th International Conference on Solid State Ionics, Hakidiki, 1999.

Table 1. Crystallographic Data for $Li_xV_2(PO_4)_3$ (x = D3.0, D2.0, D1.0, 0.0, R1.0)[a]

composition	$Li_3V_2(PO_4)_3$[b,c]	D-$Li_2V_2(PO_4)_3$[b]	D-$LiV_2(PO_4)_3$[b]	D-$V_2(PO_4)_3$[b]	R-$LiV_2(PO_4)_3$[d,e]
x/$Li_xV_2(PO_4)_3$	3.0	2.0	1.0	0.0	1.0
color	green	black	black	olive green	black
crystal system	monoclinic	monoclinic	monoclinic	monoclinic	monoclinic
space group	$P2_1/n$	$P2_1/n$	$P2_1/n$	$P2_1/n$	$P2_1/n$
a (Å)	8.606	8.457	8.301	8.407	8.308
b (Å)	8.591	8.621	8.518	8.515	8.585
c (Å)	12.036	11.896	11.653	11.590	11.386
β (deg)	90.61	90.24	89.60	89.13	89.31
V (Å^3), Z	899.8	867.2	823.8	829.6	812.1
angular range	5−116°	10−150°	10−150°	10−150°	10−150°
variables	75	72	73	54	95
R_{wp}	4.42%	4.83%	3.86%	3.55%	3.74%
R_{F^2}	6.87%	8.01%	5.60%	19.14%	6.33%
χ^2	6.87	4.80	2.94	3.96	5.13

[a] Data collected at 300 K. [b] Constraints: U_{iso} (P1) = U_{iso} (P2) = U_{iso} (P3); U_{iso} (O1) = U_{iso} (O2) = ... = U_{iso} (O12); U_{iso} (Li_1) = ... = U_{iso} (Li_n) for relevant lithium ions. [c] Refinement from data collected at the Chalk River Neutron Laboratory. [d] Constraints: U_{iso} for Li ions was fixed; fractional occupancy was fixed at NMR-derived values. [e] Restraints: initial on-bond distances: Li_1 to (O2,O4) and Li_2 to (O1, O6, O8, O12) of 2.0 ± 0.2 Å; Li_1 to (O5, O11) of 2.1 ± 0.2 Å; Li_2 to O4 of 2.5 ± 0.2 Å.

long Li−O bond and are formally five coordinate (see Supporting Information), as is depicted in Figure 2a-ii.

The local Li environments are also distinguishable by ^{7}Li MAS NMR (Figure 3). The spectrum of $Li_3V_2(PO_4)_3$ displays three well-resolved isotropic chemical shifts at 103, 52, and 17 ppm (Figure 3a) corresponding to the three crystallographic Li sites. The remainder of the peaks represent spinning sidebands resulting from the quadrupolar interaction due to the electric field gradient's nonspherical symmetry at the Li nucleus. Integration of the peak area of the isotropic bands (including its sidebands)[16] yielded a ratio of exactly 1:1:1, in accord with the crystal structure. By comparison, the rhombohedral phase of $Li_3V_2(PO_4)_3$ with the same stoichiometry containing only one unique tetrahedral Li site displays a single line at an average of these values, 85 ppm.[11]

The shift of the ^{7}Li NMR lines (as compared to the reference at 0 ppm) arises from the well-known hyperfine interaction or Fermi contact shift.[23] Partial transfer of electron density from the V^{3+} t_{2g}-like orbitals to the Li 2s orbital gives rise to a positive spin density and hence a positive shift. This has been quantified to some degree in other materials: $LiMn_2O_4$[24] and $LiMPO_4$ (M = Fe, Mn, Co, Ni).[25] The Fermi contact shift is dependent on the number of d-electrons (all d^2 in $Li_3V_2(PO_4)_3$) and the nature of the orbital overlap-interaction; hence, the Li−O−V bond lengths and bond angles determine the exact magnitude of the shift. These effects can be quite subtle, as was demonstrated in rhombohedral $Li_3Ti_2(PO_4)_3$.[26] Understanding how these parameters will affect the NMR shift in monoclinic-$Li_3V_2(PO_4)_3$, where the three Li ions all possess very different Li_n−O−V(1,2) linkages; varying Li−O−V bond angles (from 74° to 110°) and Li−O bond lengths (see Table 3), is challenging. Although it is tempting to correlate the NMR shifts with the crystallographic sites at this stage, calculations of the Fermi-contact shift interaction (currently underway) are necessary to quantify the effects.

D-$Li_{2.5}V_2(PO_4)_3$. The electrochemical curve shows the existence of a phase at x = 2.5 midway between x = 2.0 and x = 3.0 (Figure 1, inset). Because it sits on a very small voltage step on the electrochemical curve, this phase is clearly similar in energy to those on either side and hence would have an intermediate structure. In accord, a LeBail fit of the neutron diffraction (and X-ray) pattern gave lattice parameters midway between the two other phases. Subsequent Rietveld analysis coupled with ^{7}Li NMR data shows that the framework is very similar to the neighboring x = 3 and x = 2 phases, with the Li_1 site being common to all three structures and fully occupied. The Li_2 and Li_3 sites are similar to those in $Li_3V_2(PO_4)_3$ but are partially occupied. A full description of the structure solution and ^{7}Li NMR spectrum for this material, which is complex because of the presence of the Li site vacancies and multiple vanadium valencies, will be reported elsewhere.[27]

D-$Li_2V_2(PO_4)_3$. Full-pattern matching confirmed the material was single phase. A preliminary structural refinement of the X-ray powder pattern for $Li_2V_2(PO_4)_3$ revealed that the best agreement was obtained in the space group $P2_1/n$. Using the XRD data, we refined the $V_2(PO_4)_3$ framework to locate the V positions which were then fixed, and refinement proceeded with the neutron diffraction data. The Fourier difference map unequivocally revealed that residual nuclear densities remain at two sites, representing the locations of Li_1 and Li_2. All other major contour regions can be related to Li_1 and Li_2 sites by nonspecial 4e positions of the $P2_1/n$ space group. The Li-ion positions found were used as input for the Rietveld refinement, and the atomic coordinates and occupation factors were refined. Convergence was achieved for occupancy factors close to 1:1 that converged to these values in the absence of any constraints. Although the cell possesses pseudosymmetry close to that of an orthorhombic cell, the attempt to refine the cell in an orthorhombic (*Pbna*) space group resulted in higher convergence values. As is shown in Figure 4a and Table 1, an excellent final agreement was obtained between the experimental and calculated neutron diffraction patterns (R_{wp} = 4.83%).

The framework shown in Figure 2b-i is very similar to the previous two phases in terms of connectivity. The phosphate tetrahedra are slightly distorted with typical average P−O bond lengths. The environments for the slightly distorted vanadium

(23) Marichal, C.; Hirschinger, J.; Granger, P.; Menetrier, M.; Rougier, A.; Delmas, C. *Inorg. Chem.* **1995**, *34*, 1773.
(24) Lee, Y. L.; Wang, F.; Grey, C. P. *J. Am. Chem. Soc.* **1998**, *120*, 12601.
(25) Tucker, M. C.; Doeff, M. M.; Richardson, T. J.; Finones, R.; Cairns, E. J.; Reimer, J. A. *J. Am. Chem. Soc.* **2002**, *124*, 3832.
(26) Aatiq, A.; Menetrier, M.; Croguennec, L.; Suard, E.; Delmas, C. *J. Mater. Chem.* **2002**, *12*, 2971.
(27) Yin, S. C.; Grondey, H.; Strobel, P.; Nazar, L. F. *Chem. Mater.*, submitted.

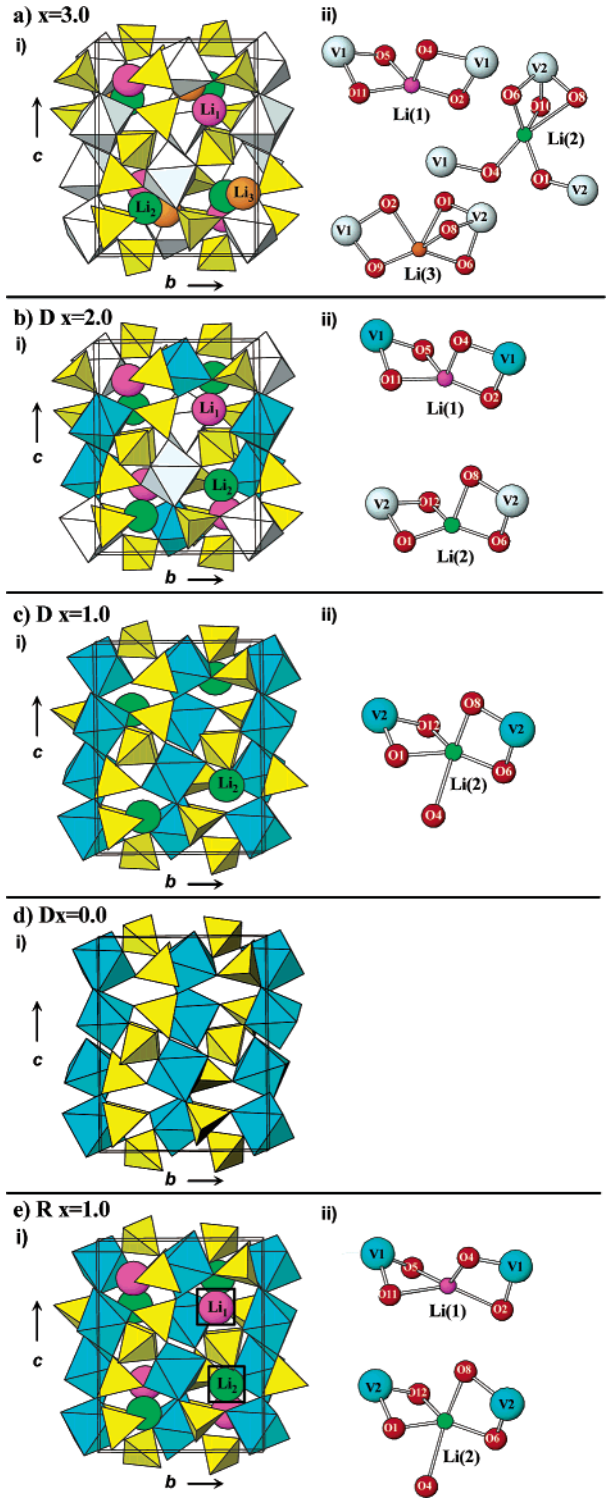

Figure 2. (a) Monoclinic $Li_3V_2(PO_4)_3$: **(**i) crystal structure. V1(V^{3+})−O and V2(V^{3+})−O octahedra are shown in gray, and P−O tetrahedra are shown in yellow. Li_1, Li_2, and Li_3 atoms are shown in magenta, green, and orange, respectively. (ii) Li coordination environments. (b) D-$Li_{2.0}V_2(PO_4)_3$: **(**i) crystal structure. V1(V^{4+})−O octahedra are shown in blue, and V2-(V^{3+})−O octahedra are shown in gray. Li_1 and Li_{2b} atoms are shown in magenta and green, respectively. (ii) Li coordination environments. (c) D-$Li_{1.0}V_2(PO_4)_3$: **(**i) crystal structure. V1(V^{4+})−O octahedra are shown in blue, and the Li_{2c} site is shown in green. (ii) Li coordination environment. (d)$V_2(PO_4)_3$: **(**i) crystal structure. ($V^{4+/5+}$)−O octahedra are shown in blue. (e) R-$Li_{1.0}V_2(PO_4)_3$: (i) crystal structure. (V^{4+})−O octahedra are shown in blue, and partially occupied sites corresponding to the Li_{1*} and Li_{2c} atoms are shown in magenta and green, respectively. (ii) Li coordination environments; the squares surrounding the sites indicate partial occupancy of the two sites.

oxygen octahedra, however, are significantly different for V(1) and V(2). The average V(2)−O bond length of 1.99 Å, typical of a V^{3+}−O bond and very similar to that in the starting phase, $Li_3V_2(PO_4)_3$, results in a calculated vanadium valence of +3.1 (see Table 2). By comparison, the shorter average V(1)−O length (1.91 Å) is characteristic of V^{4+}−O, with a calculated valence of +4.3. This charge ordering of the vanadium ions, as was communicated in our prior report,[13] is depicted in Figure 5. The V^{4+}(V^{3+})−O octahedra form "columns" of either V^{3+} or V^{4+} running along the *b*-axis, with the columns ordered as V^{3+}/V^{4+} in the (010) plane. We note that, although a few inorganic vanadium V^{4+}/V^{5+} phosphates appear to exhibit valence ordering,[28] this is the first time it has been observed in an electrochemically active phosphate, although evidence for it has been previously sought.[29] It is tempting to ascribe its existence here to the fact that V(1) and V(2) are distinguishable in the starting phase. These two ions, however, must be distinct because of the monoclinic lattice symmetry, although their difference in coordination environment is not statistically significant within the limits of the single-crystal analysis (*vide supra*).[9] Irrespective of its origin, the presence of charge ordering is highly important to charge transport within the framework. The existence of ordered valence states in $Li_2V_2(PO_4)_3$ proves that the electrons are pinned on a long (NMR) time scale (see below) as well as on a short (XRD) time scale.

Examination of the changes in the Li coordination environment shows that the five-coordinate site Li_3 in $Li_3V_2(PO_4)_3$, which is the highest energy site based on bond-sum calculations,[30] is extracted on oxidation. Two sites remain. One, Li_1, is essentially unaltered in location and geometry as compared to the pseudotetrahedral Li_1 site in $Li_3V_2(PO_4)_3$. The other site which we call Li_{2b}, as it is related to "Li_2" in the starting phase, becomes a tetrahedral site which is very similar to Li_1 (Figure 2b-ii). Not only do Li_1 and Li_{2b} have the same geometry and average Li−O bond length (Table 3), but they are pseudosymmetry sites. They would be identical if the lattice were orthorhombic. The average Li−O bond distance of 1.97 Å is the same for both sites (see Table 3). We were gratified to see first-principles calculations[19] also predict the population of these two sites; however, the orthorhombic symmetry of their lattice results in complete equivalency of the two Li ions.

The ^{7}Li NMR experiments are particularly significant, as they provide the clearest evidence for V^{3+}/V^{4+} ordering and the existence of monoclinic symmetry. The material shows two isotropic ^{7}Li NMR chemical shifts at 143 and 77 ppm (Figure 3b), in accord with the two lithium sites described above. Peak integration yields precisely a 1:1 ratio for these two, almost identical Li_1 and Li_{2b} coordination environments. Because the sites are independent − Li_1 is solely connected to $V(1)^{4+}$ and Li_{2b} to $V(2)^{3+}$ − the shift difference must be due to the one electron difference in orbital transfer between Li_1−O−V(1)d^1 and Li_{2b}−O−V(2)d^2, that is, the magnitude of the hyperfine interaction between the two sites.[31] Both shifts are positive, implying that one d-electron in a t_{2g} orbital contributes +77

(28) Koene, B.; Taylor, N.; Nazar, L. F. *Angew. Chem.* **1999**, *38*, 2888. Bontchev, R. P.; Do, J.; Jacobson, A. J. *Mater. Res. Soc. Symp. Proc.* **2001**, *658*, 7.1.
(29) Eyob, P.; Andersson, A. S.; Thomas, J. O. *J. Mater. Chem.* **2002**, *12*.
(30) Bond sum calculations for Li(1), 1.043; Li(2), 1.018; Li(3), 0.915; see: Brown, I. D. *Chem. Soc. Rev.* **1978**, *7*, 359.
(31) First-principles calculations find the same two site locations as we report here. The orthorhombic symmetry of their lattice results in the two sites being identical, however.

Table 2. Summary of Average Bond Lengths for V−O and P−O Distances in Å (See Supporting Information for Details), and Bond-Sum Calculations on the Vanadium Sites

composition	V(1)–O	calculated V valence[b]	V(2)–O	calculated V valence[b]	P(1)–O	P(2)–O	P(3)–O
[a]$Li_3V_2(PO_4)_3$	2.003	3.16	2.006	3.10	1.545	1.558	1.548
D-$Li_2V_2(PO_4)_3$	1.911	4.33	1.988	3.10	1.536	1.533	1.543
D-$LiV_2(PO_4)_3$	1.909	4.31	1.905	4.33	1.532	1.533	1.533
D-$V_2(PO_4)_3$	1.909	4.51	1.905	4.52	1.551	1.510	1.537
R-$LiV_2(PO_4)_3$	1.910	4.27	1.911	4.40	1.518	1.535	1.537

[a] Values from the single-crystal structure, ref 9 (or see CIF file). [b] Values from bond-sum calculations (Brown, I. D. *Chem. Soc. Rev.* **1978**, *7*, 359).

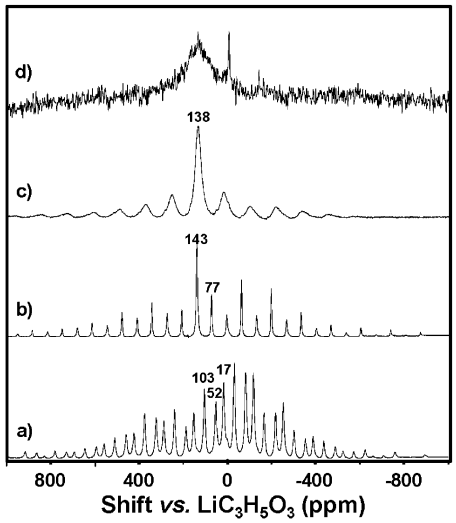

Figure 3. ^{7}Li MAS NMR spectra of $Li_xV_2(PO_4)_3$, $x = 3 \rightarrow 0$ on deinsertion; $x =$ (a) 3.0; (b) 2.0; (c) 1.0; (d) 0.0. The isotropic shift values are labeled; all other peaks are spinning sidebands. In part d, the sharp line at 0 ppm arises from minute amounts of Li salt contamination.

ppm to the shift, with the second electron contributing an additional ~66 ppm to give the shift at 143 ppm. The average contribution of one d-electron of 72 ppm is in good agreement with the value of +70 ppm for a single electron in an A″ orbital (lower symmetry than t_{2g}) in $LiMPO_4$.[25] Here, we ignore any effects of orbital splitting due to symmetry variation from pure O_h symmetry. In summary, the +77 ppm shift is assigned to Li_1 ($Li_1-O-V_1d^1$), and the 143 ppm shift is assigned to Li_2 ($Li_{2b}-O-V_2d^2$). Note that the NMR distinguishability of the two sites confirms the lattice is monoclinic, not orthorhombic.

That the effects we see here are due to the hyperfine interaction is illustrated by our temperature-dependent ^{7}Li NMR measurements performed on D-$Li_2V_2(PO_4)_3$. The results display a characteristic linear variation of both lines with reciprocal temperature that follows the expected paramagnetic susceptibility. Figure 6 shows the linear dependency of shift versus $1/T$ which follows the predicted Curie−Weiss type dependency and confirms the origin of the shift. The positive slope resembles that seen for similar materials such as $LiMnPO_4$.[25]

D-$LiV_2(PO_4)_3$. Rietveld refinement of the neutron diffraction pattern of D-$LiV_2(PO_4)_3$ (Figure 4b) followed the methodology used for the previous three phases. Guided by our ^{7}Li NMR studies that showed only one Li site in this phase (see below), we took the initial coordinates for Li from those of $Li_2V_2(PO_4)_3$ and refined them with full occupancy of either Li_1 or Li_2. The reliability factors ($R_{wp} = 3.86\%$; see Table 1) were excellent when the site Li_2 was fully occupied ("Li_{2c}" to indicate it is related to Li_2), and a very good agreement was achieved between the experimental and calculated neutron diffraction patterns. The occupancy of Li_{2c} converged to one in the absence of constraints. Partial occupancies of both sites did not result in convergence. A model of the structure is shown in Figure 2c-i, and the final refinement results are listed in Table 1. The phosphate tetrahedra show typical coordination and bond lengths (Table 2). The V(2)−O distances decrease to an average value (1.907 Å) similar to that for V(1)−O (1.908 Å), in agreement with the unique V^{4+} oxidation state. The monoclinic symmetry of the lattice is preserved, although a significant twist in the structure as compared to D-$LiV_2(PO_4)_3$ results in a five-coordinate environment for Li_2 (Figure 2c-ii). This arises from the approach of O4 (bonded to V1) to Li_{2c} in the "twisted" structure, forming an additional 2.6 Å Li−O bond (see Table 3).

The slightly shifted Li_{2c} site results in one isotropic chemical shift at 138 ppm in the ^{7}Li NMR spectrum (Figure 3c). As the previous argument suggests that a $Li-O-Vd^1$ interaction should give rise to a shift of about 77 ppm, clearly the additional fifth oxygen interaction that now provides a mechanism of electron density transfer from V(1) (or geometrical changes at the Li site) must be responsible for an additional positive contribution. An additional feature of the D-$LiV_2(PO_4)_3$ spectrum is the line broadening which may originate from local Li disorder as suggested in $LiFePO_4$.[32]

D-$V_2(PO_4)_3$. Extraction of the third Li ion/electron (upper plateau at 4.55 V) is kinetically the most difficult, as is evident from the greater deviation between transient and equilibrium voltage in the region between $x = 1$ and 0. The reasons undoubtedly lie in the reduced ionic/electronic conductivity of the fully extracted phase. Complete extraction of Li from the framework was confirmed by chemical analysis, which gave a composition of $Li_{0.08}V_2(PO_4)_3$, and ^{7}Li NMR, where no well defined ^{7}Li signal could be observed (Figure 3d). The structure of the fully emptied framework, $V_2(PO_4)_3$, was refined from the neutron diffraction pattern, starting with the parameters from the $x = 1$ phase (Figure 4c). Convergence was achieved with good reliability factors ($R_{wp} = 3.55\%$, Table 1 and Supporting Information). The framework shown in Figure 2d-i maintains monoclinic symmetry after removal of all of the lithium ions, exhibiting little alteration of the framework, with the PO_4^{3-} groups exhibiting normal distances (Table 2). V(1) and V(2) display fairly close average bond distances and average vanadium valencies of +4.5, indicating that V^{4+}/V^{5+} charge ordering does not occur in this phase (Table 2). The higher background and reduced diffraction signal/noise indicates a little loss of crystallinity in this phase, in agreement with the X-ray diffraction results (Figure 1e).

(32) Tucker, M. C.; Doeff, M. M.; Richardson, T. J.; Finones, R.; Reimer, J. A.; Cairns, E. J. *Electrochem. Solid-State Lett.* **2002**, *5*, A95.

Table 3. Li−O Bond Lengths (in Å)

D x =3	Li_1−O	O(2): 1.88(5)	O(4): 1.99(6)	O(5): 1.96(5)	O(11): 2.02(6)	
	Li_2−O	O(1): 1.94(5)	O(4): 2.08(3)	O(6): 2.00(5)	O(10): 2.13(5)	O(8): 2.73(1)
	Li_3−O	O(2): 2.08(5)	O(6): 2.07(5)	O(8): 1.84(5)	O(9): 2.02(5)	O(1): 2.39(5)
D x = 2	Li_1−O	O(2): 1.85(3)	O(4): 1.95(3)	O(5): 2.08(3)	O(11): 2.00(3)	
	Li_{2b}−O	O(1): 1.90(3)	O(6): 1.90(3)	O(8): 2.09(3)	O(12): 2.00(3)	
D x = 1	Li_{2c}−O	O(1): 2.01(2)	O(6): 1.89(2)	O(8): 2.00(2)	O(12): 2.02(2)	O(4): 2.45(2)
R x = 1	Li_{1*}−O	O(2): 2.15(2)	O(4): 2.09(3)	O(5): 2.32(2)	O(11): 2.18(3)	
	Li_{2c}−O	O(1): 1.88(2)	O(6): 1.96(2)	O(8): 2.10(2)	O(12): 2.12(2)	O(4): 2.57(1)

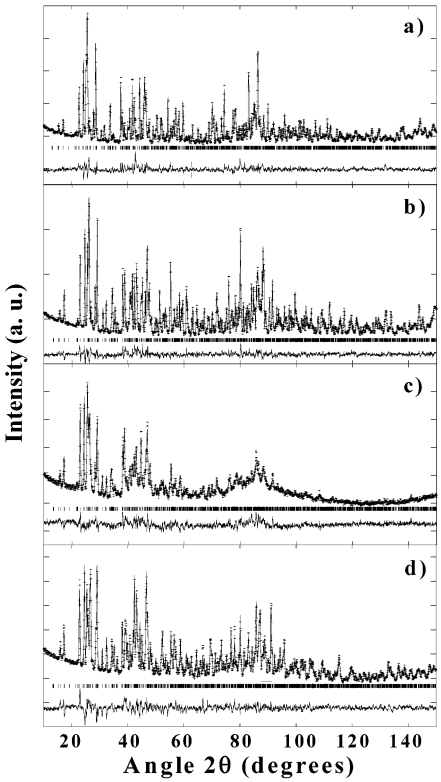

Figure 4. Comparison of the experimental (+) and calculated (−) neutron diffraction patterns for (a) D-$Li_2V_2(PO_4)_3$; (b) D-$Li_1V_2(PO_4)_3$; (c) D-$V_2(PO_4)_3$; and (d) R-$Li_1V_2(PO_4)_3$. The positions of the (*hkl*) reflections and the difference curve are also shown.

(3) Reinsertion of Lithium (Reduction Curve) − Structure Description. R-$LiV_2(PO_4)_3$. On Li insertion into the emptied $V_2(PO_4)_3$ lattice, solid solution behavior is exhibited in the electrochemical voltage−composition plot, as is indicated by the characteristic S-shaped curve. It persists until the R-$Li_2V_2(PO_4)_3$ composition is attained. Two diffraction patterns were recorded in this regime, for $x = 0.5$ and $x = 1.0$. Because of the similarity of their powder neutron patterns, we refined only one phase, $x = 1.0$ (R-$LiV_2(PO_4)_3$), to compare it to the phase on deinsertion (D-$LiV_2(PO_4)_3$, Figure 1).

The significant differences in the XRD patterns of these two materials (Figure 1) were even more apparent by neutron diffraction. The pattern and refinement for R-$LiV_2(PO_4)_3$ is shown in Figure 4d. The initial LeBail fit converged with good statistics ($R_{wp} = 2.28$ with a $\chi^2 = 1.747$), revealing that the *c*-axis in the reinserted phase (11.37 Å) is contracted as compared to the fully deinserted phase (11.65 Å). The framework atomic coordinates from the D-$LiV_2(PO_4)_3$ model were used as a starting point for the Rietveld refinement. A separate trial starting with $V_2(PO_4)_3$ produced similar results. Fourier

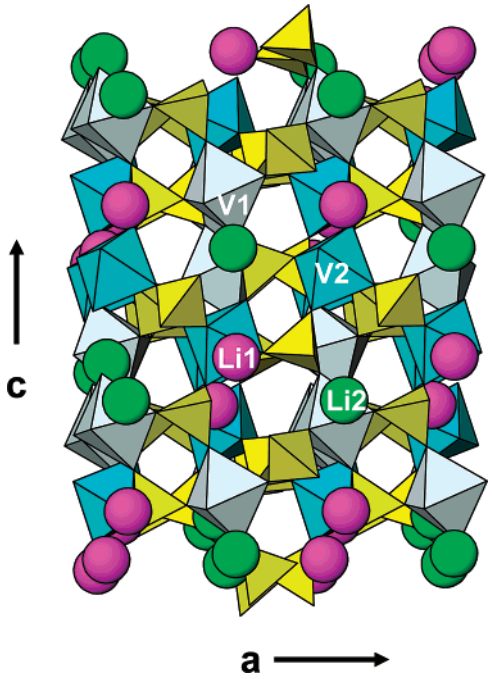

Figure 5. Columnar view of charge ordering in D-$Li_2V_2(PO_4)_3$.

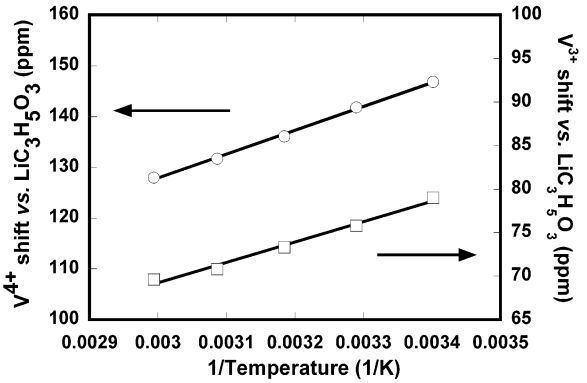

Figure 6. Temperature dependence of the two isotropic chemical shifts in D-$Li_2V_2(PO_4)_3$. Lithium lactate was used as the reference at 0 ppm.

mapping revealed that the same sole site (Li_{2c}) was not occupied as the D ($x = 1$) phase. The two sites that were located (see Figure 4 caption for details) were symmetry related to both Li_1 and Li_{2b} in the D-$Li_2V_2(PO_4)_3$ phase, and refinement was carried out with partial occupation of these sites. As the presence of one Li dispersed in two sites as a solid solution made structure solution more difficult than the other compositions, bond restraints were applied in the early stages to avoid unreasonably short Li−O bond distances. These were relaxed as the refinement progressed. The final solution achieved very good agreement between the experimental and calculated neutron diffrac-

tion patterns, and good reliability factors ($R_{wp} = 3.74\%$). The crystal structure is displayed in Figure 2e-i.

All bond lengths were refined to reasonable values, with an average V−O distance of 1.915 Å for V(1)−O and 1.912 Å for V(2)−O (typical of V^{4+}) and average P−O distances of 1.53 Å for each PO_4^{3-} group as is summarized in Table 2. As before, the $V_2(PO_4)_3$ framework is preserved with $P2_1/n$ symmetry. The simultaneous, partial occupation of both sites gives rise to the shorter *c*-axis of R-$LiV_2(PO_4)_3$ as compared to D-$LiV_2(PO_4)_3$ due to the additional Li^+−O lattice interactions. The locations of the two new Li sites are essentially the same as Li_1 in D-$Li_2V_2(PO_4)_3$ and Li_{2c} in D-$Li_1V_2(PO_4)_3$ (see Li environments Figure 2b-ii and 2c-ii), although slight differences between the frameworks result in small changes in the coordination environment.

In the reinserted $x = 1$ phase, Li_2 resides in a five-coordinate site with four average bond lengths of 2.01 Å, and a fifth longer Li−O bond of 2.57 Å (Table 3). This coordination environment is very similar to that of Li_{2c} in the corresponding deinserted phase (D-$Li_1V_2(PO_4)_3$), and it also exhibits a very similar NMR shift (see below). The Li_1 ("Li_{1*}") is in a four-coordinate site almost identical in location to that in D-$Li_2V_2(PO_4)_3$, although in this case the site is a little expanded as compared to the deinserted $x = 2$ phase, resulting in a slightly longer average Li−O distance of 2.18 Å. Partial occupation of both of these sites in R($x = 1$) is intuitively expected, because insertion of an additional 1.0 Li to give R($x = 2$) results in a diffraction pattern and NMR spectrum identical to those of D-$Li_2V_2(PO_4)_3$ (next section).

These differences in lithium occupancy between the phases on the charge and discharge curve are manifested in structural effects. The volume/unit cell parameters of the reinserted phase (R-1) are not the same as those of the delithiated phase (D-1), in accord with their nonequivalency in the electrochemical curve. If the structures were the same, there would be no hysteresis in the curve under equilibrium conditions, and the open-circuit potential of D-1 and R-1 would be the same. On complete delithiation to form $V_2(PO_4)_3$, the lattice expands by comparison to D-$Li_1V_2(PO_4)_3$. This can be easily understood by the fact that the attractive forces between the Li^+ ions (located in one Li_2 site in D-$Li_1V_2(PO_4)_3$) and the negatively charged framework $[V_2(PO_4)_3]^-$ are lost on lithium extraction/oxidation. Notably, reinsertion of the Li^+ ions to form R-$Li_1V_2(PO_4)_3$ causes recontraction of the unit cell slightly beyond that in the D-1 phase, because the Li^+ ions are inserted in two sites, and not one, in the lattice.

(4) Reinsertion of Lithium (Reduction Curve) − Solid State NMR Study. To monitor the Li insertion process in the solid solution region by ^{7}Li NMR, a series of compositions $x = 0.5, 0.75, 1.0, 1.25, 1.5, 2.0$ in $Li_xV_2(PO_4)_3$ were prepared. Their spectra are shown in Figure 7. The conclusions drawn from this study correlate well with the structure analysis. There are two dominant isotropic chemical shifts at 134 and 75 ppm that resemble the Li_{2c} shift in D-$LiV_2(PO_4)_3$ and the Li_1 shift in D-$Li_2V_2(PO_4)_3$ (the origin of additional minor peaks in the spectrum in the first stages of reinsertion is discussed below). The summary for the NMR data for all of the phases is presented in Table 4. The contribution of the isotropic shifts in the reinsertion series of phases, summarized in Table 5, was determined by integrating the area of each isotropic shift

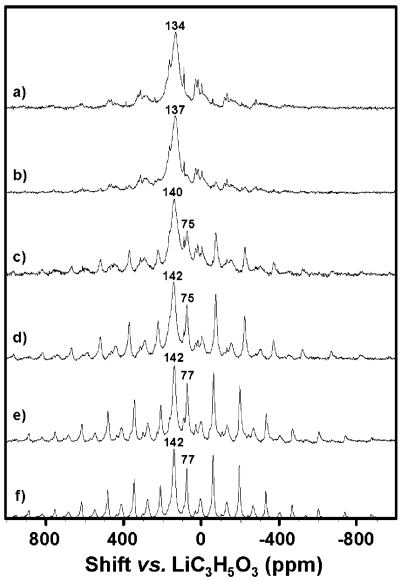

Figure 7. ^{7}Li MAS NMR spectra of R-$Li_xV_2(PO_4)_3$, $x = 0 \rightarrow 2$ on reinsertion; $x =$ (a) 0.5; (b) 0.75; (c) 1.0; (d) 1.25; (e) 1.5; (f) 2.0.

Table 4. Summary of Major ^{7}Li NMR Shifts in $Li_xV_2(PO_4)_3$ ($x =$ 3.0, D2.0, D1.0, R1.0)

phase	shifts (ppm)		
$Li_3V_2(PO_4)_3$	103	52	17
D-$Li_2V_2(PO_4)_3$	143	77	
D-$LiV_2(PO_4)_3$	138		
R-$LiV_2(PO_4)_3$	140	75	

Table 5. Area Percentage (%) of Isotropic Shift Peaks for R-$Li_xV_2(PO_4)_3$

x	182 ppm	166 ppm	142–134 ppm	92 ppm	75 ppm	32 ppm	0 ppm
0.5	9.3	9.3	71.7	3.0	0.0	3.5	3.2
0.75	6.2	10.9	65.6	2.9	10.7	0.7	3.0
1.0	0.0	4.3	55.6	1.2	32.6	6.4	0.0
1.25	0.0	5.5	44.7	1.2	46.8	1.9	0.0
1.5	0.0	4.8	41.7	3.0	50.6	0.0	0.0
2.0	0.0	2.0	44.8	0.5	52.7	0.0	0.0

including all sidebands. Multiplying each value by the corresponding Li content in each sample provides the fractional occupancy of each site. Figure 8a shows the change in distribution among the major sites on reinsertion of Li from $x = 0 \rightarrow 2.0$. Examination of the spectral sequence and the occupancy plot shows that reinsertion into the $V_2(PO_4)_3$ framework first results in a broad band at 134 ppm that strongly resembles the isotropic peak for D-$Li_1V_2(PO_4)_3$ (Figure 3c). The other peak at 77 ppm just becomes resolvable at $x = 0.75$ Li and slowly increases in intensity as Li insertion progresses. Beyond the crossover point at $x = 1.25$, the sites that correspond to these peaks are filled at the same rate, to reach 1.0 and 0.9 in occupancy at $x = 2.0$ (R-$Li_2V_2(PO_4)_3$). Furthermore, along the solid state regime from $x = 0.5-2.0$, the 134 ppm peak gradually shifts to 143 ppm (Figure 8b) and narrows in line width. This results in a spectrum for R-$Li_2V_2(PO_4)_3$ that is almost the same as that for D-$Li_2V_2(PO_4)_3$ (Figure 8c). The presence of a very minor component in the NMR spectrum of the reinserted phase is due to a small degree of site-population "irreversibility" (i.e., either presence of vacancies in the 77 ppm site or localization of V^{n+} valence states that are not exactly in the same configuration as in D-$Li_2V_2(PO_4)_3$). Recall that the

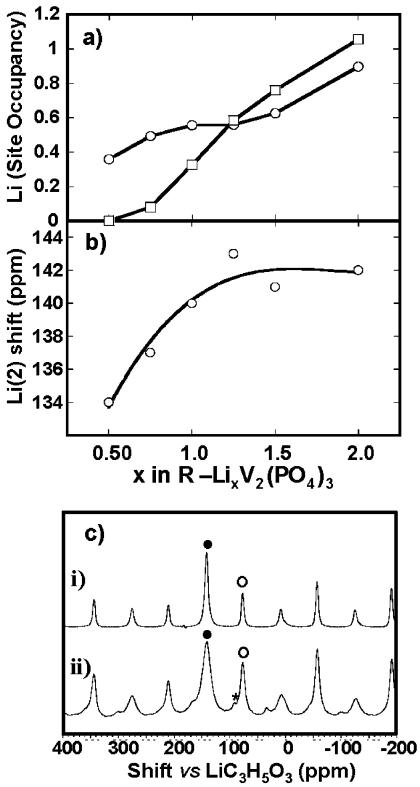

Figure 8. (a) Site occupancy of each chemical shift contribution versus Li content, corresponding to reinsertion of R-$Li_xV_2(PO_4)_3$; Li_2 at 134−142 ppm is indicated by (○-○-○), Li_1 at 75−77 pm is indicated by (□-□-□). (b) Variation of the chemical shift for site Li_2 as a function of x in R-$Li_xV_2(PO_4)_3$ ($x = 0 \rightarrow 2$). (c) Comparison of the ^{7}Li MAS NMR spectra for (i) D-$Li_{2.0}V_2(PO_4)_3$; (ii) R-$Li_{2.0}V_2(PO_4)_3$; the presence of the minor component is denoted by the asterisk.

X-ray patterns of these two phases (Figure 1c,g) are also identical, confirming that the same global structure is reached at $x = 2.0$. However, NMR can reveal subtle structural differences as it is a very sensitive probe of the local ^{7}Li environment.

We assign the peak at 134 ppm (Figure 7) to "Li_{2c}" in the neutron diffraction analysis (i.e., Li_{2c}−O−V(d^1) on the basis of its line-shape similarity, coordination environment (Figure 2c, e-ii), and shift value, to Li_{2D} in D-$Li_1V_2(PO_4)_3$ (at 138 ppm, Figure 3c). The progressive modification in the NMR shift from 134 to 143 ppm results from the subtle framework transformations in the solid solution regime. These reconfigure the Li_{2c} site to an environment that is the same as the Li_{2b} site in D-$Li_2V_2(PO_4)_3$ ("D($x = 2$")), just as the Li_{2b} site in D($x = 2$) transforms to the Li_{2c} site in D(x =1) in the opposite direction on deinsertion. Accompanying the shift from five-coordinate to tetrahedral environment in moving from R1.0 to R2.0 is the reduction of the vanadium site from V^{4+} to V^{3+}. Note that the 75 ppm shift remains almost constant (shifting to 77 ppm); it is assigned to the Li_{1*} site. This site becomes Li_1 (Li_1−O−V(1)-d^1) at the end of the solid solution regime as the site contracts upon framework alteration.

The minor shift contributions at 182 and 166 ppm showed a strong decrease from $x = 0.5$ to 1.0, which suggests the signals are either from mixed V^{4+}/V^{5+} contact shifts (i.e., a Li that is bonded to both V^{4+} and V^{5+}) or from vacancy effects as noted above. The shifts at 92 and 32 ppm generally contribute less than 3%, which is probably due to a contact shift from minor electron localization (V^{3+}/V^{4+}) in the structure.

Scheme 1. Scheme Illustrating the Mechanism Responsible for the Hysteresis in the Oxidation and Reduction Portions of the Electrochemical Curve on Extraction and Reinsertion of Li in $Li_xV_2(PO_4)_3$, between $x = 2 \rightarrow 0$

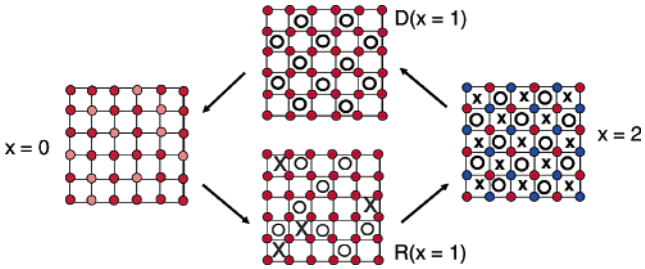

(5) Explanation for the Hysteresis. A schematic diagram which illustrates the changes in the lattice valence and site population is presented in Scheme 1. Starting with the D($x =$ 2) phase, the vanadium charge ordering is coupled with the lithium site ordering as was previously noted. On extraction of a lithium ion, one site is preferentially emptied due to the V^{4+}- -Li^+ cation repulsion. Hence, at D($x = 1$), the ordering on the lithium sites remains, although the vanadium ions are all the same valence. Full extraction of the lithium and oxidation of the lattice to a $V^{4+/5+}$ state results in a different lattice, in which no charge ordering is exhibited (Scheme 1, left). Thus, reinsertion of Li yields disorder over two sites in the absence of vanadium charge ordering. The latter effectively gives rise to more than one specific site for Li reinsertion, and hence both sites are statistically populated, resulting in a solid solution regime. The low degree of Li^+ incorporation distributed over two sites, and the low population of variable vanadium valence states, screen any possible forces that could drive ordering. Beyond $x = 1.25$, however, ordering is reestablished due to the additional contributions to the lattice potential formed from the incorporation of both Li^+ and reduced vanadium. Thus two-phase behavior is reasserted. This "disorder−order" transition is thus driven by changes in the lattice stoichiometry and metastable lattice energy effects. It is interesting to recall that since both stoichiometries D-$Li_1V_2(PO_4)_3$ and R-$Li_1V_2(PO_4)_3$ must have the same free energy, the formation of one versus the other on the oxidation and reduction curve is governed by kinetics.

Conclusions

Electron ordering plays a major role in electron transport and is a critical factor for any electrode material. The existence of ordered valence states in $Li_2V_2(PO_4)_3$ demonstrates the electrons are pinned on both long and short time scales. This may also be true for the other single-phase compositions where direct evidence cannot be obtained. Each plateau in the V versus x curve corresponds to a two-phase transition involving the reorganization of electrons and Li ions within the lattice. The structures spanning the phase transition are energetically different, governed by the site potential of the Li^+ ion and interaction with the V^{n+} ions in the lattice.

Our results suggest that Li-site ordering and the electron ordering are inextricably coupled, resulting in paired electron/ion transport in the deinsertion regime. The solid solution regime on reinsertion (from $x = 0$ to $x = 2.0$) appears to be a consequence of the mixed V^{4+}/V^{5+} state in $V_2(PO_4)_3$ formed

on complete emptying of the lattice, which does not display charge ordering. Therefore, lithium insertion results in disorder (in the absence of V^{n+} ordering to drive Li^+ ordering) until sufficient Li^+ repopulation and vanadium reduction occur. At the composition $Li_2V_2(PO_4)_3$ which signals the reappearance of two-phase behavior in the reinsertion curve, strong forces based on a combination of $V^{n+}-V^{n+}$ and $V^{n+}-Li^+$ interactions constrain the $V^{3+/4+}$ ordering within the lattice.

Our findings explain the complex steps displayed in the voltage versus composition curves of $Li_{3-x}V_2(PO_4)_3$ and are also directly relevant to other materials. In particular, they bear on the principle of using valence substitution to drive the formation of solid solution regimes. For example, the solid solution γ-phase of $Li_3V_2(PO_4)_3$, normally only accessible above 450 K, is stabilized at room temperature by the addition of a M^{4+} dopant such as Zr^{4+} to form $Li_{3-x}(V_{1-x}Zr_x)_2(PO_4)_3$. In the context of our study, it is apparent that the higher-valent dopants raise the energy of the fully charge-ordered $Li_2V_2(PO_4)_3$ on lithium extraction, and hence disordered population of the Li^+ sites results. The establishment of solid solution regimes is important to the practical implementation of these phosphates as electrode materials. This inhibits jumps in the voltage−composition curve which are problematic for device applications. Second, energy loss/kinetic impediment via hysteresis from phase boundary migration is minimized. It is also interesting to speculate on the driving force for the lack of a solid solution in Li_xFePO_4 either on oxidation or on reduction. The existence of a well-defined phase transition between $LiFePO_4$ and $FePO_4$ is undoubtedly in part due to size differences between Fe^{2+} and Fe^{3+} that also cause a 7% change in volume between the two phases. Nonetheless, lattice interactions between Li^+-Fe^{2+} that are weaker for Li^+-Fe^{3+} (no ligand field stabilization energy) would also be contributing factors that could raise the energy of the solid solution phase.

Acknowledgment. We thank the Institut Laue-Langevin, Grenoble, France, and E. Suard (ILL) for her able assistance. The NPMR at the Chalk River Facility, Canada, provided facilities for the initial neutron diffraction experiments and the assistance of R. Hammond. We are grateful to W. P. Power (Waterloo) for helpful discussions. S.-C.Y. thanks Dr. V. Pralong and Dr. S. Herle for useful discussions. L.F.N. acknowledges NSERC for funding the research program, the CNRS (Grenoble) for a visiting professorship, and is grateful to the Canada-France Foundation for providing travel funds.

Supporting Information Available: Summary of the structure refinements,; bond lengths and selected angles are reported in the tables for the compounds listed in Table 1 (PDF and CIF). This material is available free of charge via the Internet at http://pubs.acs.org.

JA034565H